Optimal flapping strokes for self-propulsion in a perfect fluid

Shane D. Ross

***Abstract*— Some animals rely on flapping a symmetrical pair of jointed appendages to generate locomotion in a fluid. We consider a simple model of the motion of such an animal propelling itself via cyclic flapping strokes in a perfect fluid. Furthermore, we determine which strokes yield the greatest locomotive efficiency, defined as those which minimize the control effort per unit distance traveled.**

I. INTRODUCTION

Some animals rely on the flapping of a symmetrical pair of articulated appendages to generate locomotion in a fluid, such as labriform fish and frogs [6], [7]. In the aquatic context, this propulsion mode is known as flapping aquatic flight [29].

In order to provide a common analytical and computational framework in which to understand the fundamentals of locomotion and design of these animals and possible biologically-inspired robotic analogues, we take the point of view of developing a family of simplified practical models, beginning with the simplest initial models and moving to more realistic, complex models [27]. For an initial model, we assume an ideal, incompressible and irrotational fluid for all time, allowing us to assume potential flow. Following [15], [22], and [14], who studied the movements of carangiform fish, we model a flapping animal as consisting of N bodies submerged in the fluid, connected via ball-and-socket or hinge joints in order to obtain a system of articulated rigid links.

Consider the symmetrical four-link flapper shown in Fig. 1. As [23] first showed, a deforming body such as this

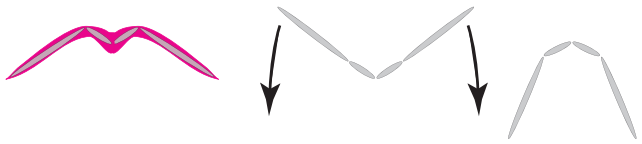

Fig. 1. A flapper in a fluid can propel itself from rest by going through periodic shape changes, an example of holonomy drive.

flapper can move persistently from rest through a perfect fluid, without having to produce vorticity in the fluid, by going through periodic changes in shape, which we generally call the stroke. Starting from rest, the multi-jointed animal changes its shape by applying internal torques at its joints. This shape actuation sets the surrounding fluid into motion, and the coupling between the shape dynamics and the surrounding fluid causes the net locomotion of the animal; the transfer of momentum between the animal's multi-link body and the fluid. This form of propulsion is fundamentally different from, say, a flapping wing for aerial flight which produces thrust in a viscous, rotational theory,

For the flapper pictured in Fig. 1, strokes are described by closed loops in the shape space, the space of allowable hinge angles. In potential flow, the net locomotion of the flapper can be formulated as a function of the stroke curve only. In other words, the net displacement of the flapper after one stroke is a function of the geometry of the loop in shape space only, and is independent of the instantaneous velocity along the loop. Thus, the locomotion of the flapper is an example of the mechanical concept of "holonomy drive" seen in many other contexts [17], including self-propulsion of microorganisms at low Reynolds number [1], [25].

A. Organization of Paper

We first describe the setting of the problem and write the Lagrangian for the motion, which is the kinetic energy of the fluid and articulated body. The net locomotion over one cycle is then determined to be a function of stroke loops in shape space. In order to determine the most efficient locomotion, we formulate an optimization problem for finding the flapping stroke loop which minimizes a certain functional.

II. THE MOTION OF A FOUR-LINK FLAPPER IN A PERFECT FLUID

Consider an articulated body of four rigid links joined by hinges, shown in Fig. 2 [21], [28]. A symmetrical flapper is one which flaps with perfect bilateral symmetry. A symmetrical flapper with only two or three links cannot achieve net locomotion in a perfect fluid. This is because no net locomotion can be achieved via reciprocal shape changes, by which is meant a motion where the body changes into a certain shape and goes back to the original shape by going through the sequence in reverse. Non-reciprocal shape changes are also required for locomotion in the low Reynolds

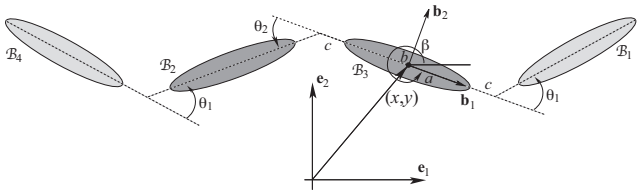

Fig. 2. A symmetrical four-link flapper immersed in an inviscid, incompressible, and irrotational fluid.

This work was supported by NSF-DMS 0402842

S. D. Ross is with the Department of Aerospace & Mechanical Engineering, University of Southern California, Los Angeles, CA 90089, USA s.ross@usc.edu

number realm [6]. Another reason four links are considered is that they provide enough degrees of freedom to approximate simple jointed appendage movements.

We approximate the four links as identical, having a slender ellipsoidal geometry with semi-major axis a and semi-minor axis b, where $b/a \ll 1$. For this initial study, we assume neutral buoyancy. The links are considered to be made of a homogeneous material of density ρ_s equal to the fluid density ρ_f. We let the joints be placed a small distance c away from the tips of the masses rather than at the tips to avoid singularities in the model which are immaterial to our analysis. We consider the joints to be equipped with muscles which generate torques to achieve a desired stroke. The four-link body is immersed in a fluid where we have potential flow and we assume the fluid particles may slip across the boundary of the body. Under these conditions, it is well known in fluid mechanics that the equations governing the motion of the body can be written without explicitly incorporating the fluid variables. That is, we can write the equations of motion of the body in terms of the body variables only, leading to significant simplification of the analysis and computation. It is perfectly appropriate in the case of studying locomotion since we are mainly interested in the location of the animal, not the fluid particles.

Consider a fixed inertial frame $\{\mathbf{e_1}, \mathbf{e_2}\}$ which spans the plane of motion as in Fig. 2. Likewise, consider four body-fixed frames $\{\mathbf{b_1}, \mathbf{b_2}\}$ attached to the center of mass of each link. Referring to the figure, let θ_2 denote the relative orientation of the two inner links. Assuming symmetric flapping, we let θ_1 denote the relative orientation of the two outer links with respect to the two inner links. These variables, which describe the shape of the body, are the shape variables. They describe only the relative orientation of the connected links, that is, the articulated body's shape. Let (β, x, y) denote the orientation and location of one of the bodies, $\mathcal{B}_3$, relative to the inertial frame. It is clear that the configuration of the articulated body can be fully described by the five variables $(\beta, x, y, \theta_1, \theta_2)$.

There is an elegant geometric description of the motion from the point of view of geometric mechanics [17]. Letting $g(t) = (\beta(t), x(t), y(t))$, it can be shown that if the shape variables $\theta(t) = (\theta_1(t), \theta_2(t))$ trace out a closed loop in shape space from time 0 to T, then the net locomotion achieved, $g(T) - g(0)$, is a function of this loop only (as shown in the appendix). We show this schematically in Fig. 3. Our goal is to use this property to investigate the loops in shape space which achieve the most efficient locomotion.

A. The Solid-Fluid Lagrangian and the Equations of Motion

As we neglect gravity under the neutral buoyancy assumption, the solid-fluid Lagrangian is the sum of the kinetic energies of the solid links and the fluid,

$$L = \sum_{i=1}^{4} T_{\mathcal{B}_i} + T_f. \tag{1}$$

The velocity of the link $\mathcal{B}_i$ with respect to the $\mathcal{B}_i$-fixed frame is $\xi_i = (\Omega_i, v_i)^T$, where Ω_i and $v_i = (v_{xi}, v_{yi})^T$ are

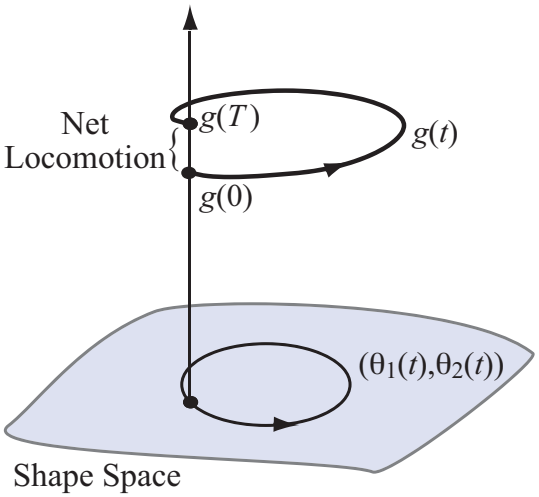

Fig. 3. As the flapper completes one stroke loop of period T in the shape space of variables (θ_1, θ_2), a net locomotion of the body, $g(T) - g(0)$, is achieved.

the angular and linear velocities, respectively. For example, $\Omega_3 = \dot{\beta}$ and $v_3 = (\dot{x}\cos\beta + \dot{y}\sin\beta, -\dot{x}\sin\beta + \dot{y}\cos\beta)^T$. The kinetic energy of the links can be written as

$$T_{\mathcal{B}_i} \;=\; \frac{1}{2}\xi_i^T\, \mathbb{I}^s\, \xi_i \;, \qquad i = 1, 2, 3, 4, \tag{2}$$

where $\mathbb{I}^s$ is the 3×3 diagonal solid inertia matrix with diagonal entries (I, m, m) where $I = m(a^2 + b^2)/4$ is the moment of inertia and $m = \rho_s \pi a b$ the mass of each ellipse.

For potential flow, the fluid velocity can be written as the gradient of a potential function, $u = \nabla\phi$, where ϕ is the solution to Laplace's equation $\nabla^2\phi = 0$ subject to the boundary conditions that the fluid is at rest at infinity and can slip across the boundary of the solids. Following a standard procedure [4], [14], the kinetic energy of the fluid can be written as

$$T_f \;=\; \frac{1}{2}\sum_{i=1}^{4}\sum_{j=1}^{4} \xi_i^T\, \mathbb{I}_{ij}^f\, \xi_j, \tag{3}$$

where $\mathbb{I}_{ij}^f$ is the 3×3 added inertia matrix.

The solid-fluid Lagrangian is then given by the total kinetic energy

$$L \;=\; \frac{1}{2}\sum_{i=1}^{4}\sum_{j=1}^{4} \xi_i^T\, \mathbb{I}_{ij}\, \xi_j, \tag{4}$$

where $\mathbb{I}_{ij} = \mathbb{I}^s + \mathbb{I}_{ij}^f$. As we take the elliptical links to be slender, we make the simplifying assumption that the added inertia associated with a given link is not affected by the presence of the other links, then $\mathbb{I}_{ij} = \mathbb{I}$ is the same for all i, j. Furthermore, $\mathbb{I}$ is diagonal with entries $(J, m_1, m_2) = (I + I^f, m + m_1^f, m + m_2^f)$, where I^f, m_1^f, and m_2^f are given by (see, e.g., [19]),

$$I^f \;=\; \rho_f\, \pi(a^2 - b^2)^2/8 \;, \qquad m_1^f \;=\; \rho_f\, \pi b^2 \;, \qquad m_2^f \;=\; \rho_f\, \pi a^2.$$

Consequently, ((4) simplifies to

$$L \;=\; \frac{1}{2}\sum_{i=1}^{4} \xi_i^T \,\mathbb{I}\, \xi_i, \tag{6}$$

The Lagrangian is a function of the five variables $(\beta, x, y, \theta_1, \theta_2)$, written in shorthand as (g, θ), where $g = (g_1, g_2, g_3)$. Therefore the equations of motion are given by the following five forced Euler-Lagrange equations [18],

$$\frac{d}{dt}\left(\frac{\partial L}{\partial \dot{g}_i}\right) - \frac{\partial L}{\partial g_i} \;=\; 0, \qquad i = 1, 2, 3, \tag{7}$$

$$\frac{d}{dt}\left(\frac{\partial L}{\partial \dot{\theta}_i}\right) - \frac{\partial L}{\partial \theta_i} \;=\; \tau_i, \qquad i = 1, 2, \tag{8}$$

where the internal torques $\tau(t) = (\tau_1(t), \tau_2(t))$ are exerted by actuators (or muscles) associated with the joints, by which the flapper changes its shape.

B. The Flapping Stroke

Flapping flight results from a periodic change of shape. A flapping stroke is a closed path in the shape space, parametrized by time, as shown in Fig. 3. If we denote the shape space as Θ, then a stroke is a curve $\gamma(t),\ 0 \le t \le T$, in Θ, where T is the period of the stroke. When a flapper has completed one stroke, it is back to its original shape, but has translated a distance $D(\gamma)$ and may be rotated. In the case of a symmetrical flapper, the rotation after each cycle vanishes. Reparametrization with respect to time constitutes an equivalence relation on the set of strokes; a stroke class $[\gamma]$ contains all strokes which determine the same loop in Θ.

To compute the flight distance $D(\gamma)$ over one flapping cycle, we solve (7) for a given stroke. As shown in the appendix, the flight distance is a function only of the loop in Θ and is independent of the time parametrization, i.e., $D(\gamma) = D([\gamma])$.[1] In other words, the distance traveled in one cycle does not depend on the instantaneous speeds along the loop. The net locomotion is an example of a geometric phase and depends only on the geometry of the loop γ (see, e.g., [15], [17]). However, the torque effort,

$$W(\gamma) \;=\; \int_0^T |\tau|^2 \, dt, \tag{9}$$

does depend on the velocities along the loop, where τ comes from solving (8).

III. Optimal Flapping

For fixed body parameters a, b, c, densities $\rho_s = \rho_f$, and stroke period T, optimal flapping comes from minimizing the torque effort per unit distance travelled, $W(\gamma)/D([\gamma])$. Therefore we want to find strokes γ which minimize $\delta(\gamma) = W(\gamma)/D([\gamma])$, a measure of inefficiency for the stroke.

[1]We note that due to the time reversibility of the problem, going through the same stroke in reverse yields the same net distance travelled, but in the opposite direction.

A. Admissible Shape Space

The appendages of the four-link flapper cannot self-intersect. This imposes boundaries in the space of variables (θ_1, θ_2). If we consider the limit of thin ellipses, $b/a \ll 1$, then the admissible shape space Θ is the subset of the square $[-\pi, \pi] \times [-\pi, \pi]$, such that $|\theta_1| + |\theta_2| \le \pi$ as shown in Fig. 4. Admissible strokes (assumed hereafter) are closed paths γ that lie in the admissible shape space.

B. Optimization

Our goal is to find the loop γ which minimizes $\delta(\gamma)$ subject to the equations of motion (7-8). This is a standard problem in optimization. By discretizing τ, g, and θ, it becomes a finite dimensional nonlinear optimization problem, which can be solved to find the nearest local minimum by standard methods like sequential quadratic programming, used in this study [11], [12], [13], [24].

The shape variables (θ_1, θ_2) which trace out γ are given by the input torques (τ_1, τ_2). Therefore, we seek the torque profile $\tau(t)$ which minimizes $\delta(\gamma)$. The minimizer of $\delta(\gamma)$ can be computed numerically as follows. The loop which minimizes $\delta(\gamma)$ is independent of a, T, c or the densities (since their ratio is 1), so we set $a = T = \rho_s = 1$ and $c = 0$ without loss of generality. We pick $b/a = 0.1$. We also pick a simple elliptical loop γ_{init} as an initial guess for the optimization scheme.

We find that there are many local minima, as is common in optimization problems. By scanning over many initial guess loop sizes and positions, we obtain an approximate globally optimal stroke which is shown in Fig. 4. Snapshots of the corresponding flapping motion are shown in Fig. 5. The irregular shape of the optimal stroke is due to the nonlinear nature of the problem. Another view of the optimal stroke is

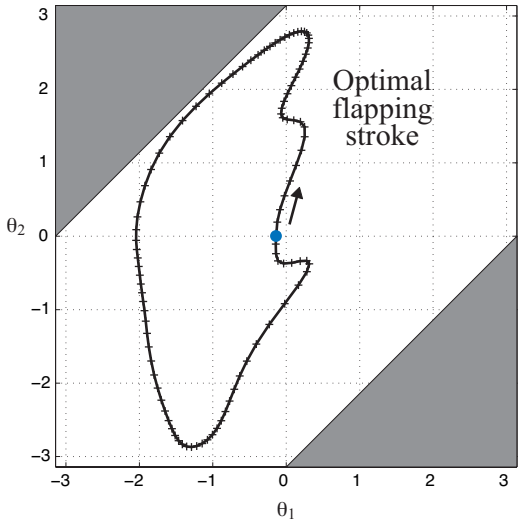

Fig. 4. The white region is the admissible shape space (no self-intersection of the links). The globally optimal stroke is shown. The arrow indicates the direction of motion. Tick marks are equally spaced in time and indicate the instantaneous speeds along the stroke. The irregular shape of the optimal stroke is due to the nonlinear nature of the problem.

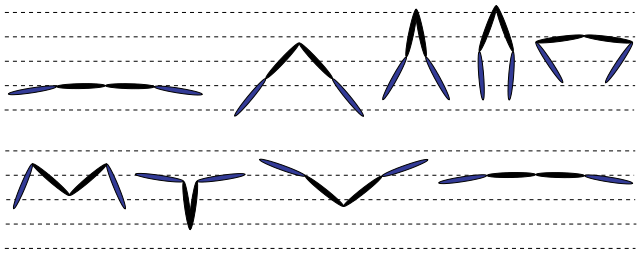

Fig. 5. Snapshots of the optimal flapper shifted horizontally for visibility. Going from the upper left to the lower right, the snapshots are separated by $T/8$. The first and last snapshots are related by a vertical translation, obtained by traversing the stroke loop in Fig. 4(a) in a counterclockwise manner, starting and stopping at the point marked with a dot. The full movie of the motion can be found on the web at `http://shaneross.com/movies/optimalflapper.mpg`.

given by plotting the appendage tip trajectory viewed from the middle joint of flapper in Fig. 6(a). Interestingly, from Figs. 5 and 6(b) we see that the location of the middle joint of the four-link flapper over the course of the stroke reaches a maximum distance greater than $D(\gamma)$ and a minimum less than the starting position before reaching $D(\gamma)$ at the end.

IV. DISCUSSION AND EXTENSIONS

The optimal flapper found is optimal under the assumptions of the model, most significantly, that irrotational flow prevails. Simple extensions of the model would involve consideration of other small aspect ratios b/a, non-identical links, additional links, and, for purposes of steering, relaxing the assumption of symmetrical flapping. Enlarging the class of flappers would allow for systematic exploration of possibly superior flappers that may use quite different styles.

In the high Reynolds number realm applicable to birds, insects, fish, and swimming mammals, one commonly envisages flapping locomotion occurring via mechanisms for producing thrust and lift through vortex shedding and interactions of the organism and its appendages with the shed vorticity. Of course, animals in nature do interact with vortices shed by the animal itself or generated by other moving organisms or fixed obstacles. Recent experimental evidence shows that fish, for example, prefer to exploit circulation in the flow to reduce their locomotion costs [16]. But the computations shown here demonstrate that vortex shedding is not solely responsible for the locomotion, as noted earlier in [23].

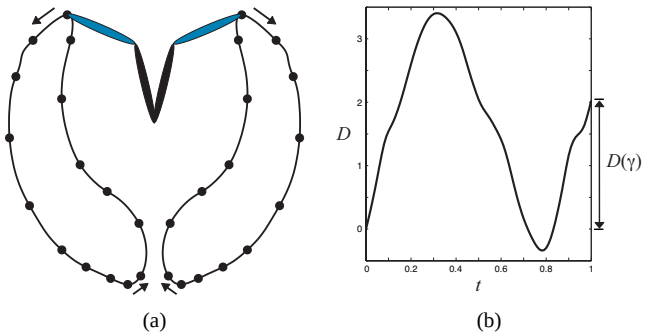

Fig. 6. (a) The path of the appendage tips of the optimal flapper, with respect to the middle joint (the center of the four-link flapper). Arrows indicate the direction of appendage tip movement and filled circles indicate the position of the tips at snapshots separated by $T/15$. (b) The distance traveled by the middle joint as a function of one period for the optimal flapping stroke.

Nevertheless, understanding how these animals and their man-made vehicle analogues behave in the presence of vortices is essential to studying their locomotion and stability. For this reason, the present study of locomotion in potential flow is viewed as the first step in the generation of a family of models that will eventually treat the interaction of multi-link vehicles with self-generated vortices and vortices shed by other objects. Therefore, another future extension is the incorporation of vorticity in a model which maintains the simplicity of the current one, i.e., including the effects of the fluid without explicitly incorporating the fluid variables. A model which incorporates the interaction of an articulated body in an inviscid and incompressible fluid with point vortices would be a good start [3], [20], [26]. This would allow for the incorporation of a lift force to counteract gravity, which needs to be incorporated into future models for situations where neutral buoyancy is a poor approximation. The evolution of the optimal flapping stroke as gravity and vorticity are added could then be explored. For the study of moderate Reynolds number flows, as in the case of insects, meshing the current computational point of view with other computationally efficient tools may be considered (e.g., the viscous vortex method of [10]).

Future work should also consider other optimality criteria. When moving in a peaceful environment, an autonomous vehicle may desire to minimize control effort, as explored here. But if attacked, for example, minimizing the time to escape may become the measure of optimality. A rigorous foundation for selecting locomotion optimality criteria depending on the vehicle's immediate environment is needed. It would be of great benefit to incorporate simplified models such as the one introduced here into an integrative view of autonomous vehicle and animal motion, where the goal is to understand the sensory and mechanical feedback loops [8].

Once we consider multiple self-propelling vehicles, future work could consider how swarms of such vehicles may be controlled [5] and utilized for tasks such as distributed sensing [30], as well as the natural benefits that may result from flocking behavior [9].

V. ACKNOWLEDGMENTS

I thank G. Spedding, E. Kanso, J. Melli-Huber, P. Newton and J. Marsden for helpful discussions. This work was partially supported by the NSF grant DMS 0402842.

APPENDIX

When the motion starts from rest, (7) can be conveniently written in the following form [2], [14], [15],

$$\dot{\mathbf{g}} = -\mathbf{g}A(\theta)\dot{\theta}, \tag{10}$$

where $\mathbf{g}$ is an element of SE(2), the group of rotations and translations in $\mathbb{R}^2$, related to $g = (\beta, x, y)$ via

$$\mathbf{g} = \begin{pmatrix} \cos\beta & -\sin\beta & x \\ \sin\beta & \cos\beta & y \\ 0 & 0 & 1 \end{pmatrix} .$$

The matrix A is a function of the shape variables only. We can view the net locomotion over a stroke, $\mathbf{g}(T) - \mathbf{g}(0)$, as a geometric phase associated with the closed loop $\gamma : [0, T] \to \Theta$, where, solving (10), we get

$$\mathbf{g}(T) = \mathbf{g}(0) \exp\left(- \int_0^T A(\gamma(t)) \ \dot{\gamma}(t) \ dt \right) .$$

By Stokes' theorem,

$$\mathbf{g}(T) = \mathbf{g}(0) \exp\left(- \int_S dA(\theta) \right) .$$

where S is the region of Θ whose boundary is the loop γ (see Figs. 3 and 4). Thus, the net displacement of the flapper after one stroke is a function of the region in shape space bounded by the loop, and is independent of the instantaneous velocity along the loop.

REFERENCES

[1] Avron, J. E., Gat, O., Kenneth, O., 2004. Optimal swimming at low Reynolds numbers. *Physical Review Letters* 93, 186001.

[2] Bloch, A. M., Krishnaprasad, P. S., Marsden, J. E., Murray, R. M., 1996. Nonholonomic mechanical systems with symmetry. *Arch. Rat. Mech. Anal.* 136, 21–99.

[3] Borisov, A. V., Mamaev, I. S., 2003. An integrability of the problem on motion of cylinder and vortex in the ideal fluid. *Reg. and Chaotic Dynamics* 8, 163–166.

[4] Cendra, H., Marsden, J. E., Ratiu, T. S., 2001. *Lagrangian reduction by stages*. Vol. 152 of Memoirs. American Mathematical Society, Providence, RI.

[5] Chang, D. E., Shadden, S., Marsden, J. E., Olfati-Saber, R., 2003. Collision avoidance for multiple agent systems, in *Proc. CDC* 42, 539–543.

[6] Childress, S., Dudley, R., 2004. Transition from ciliary to flapping mode in a swimming mollusc: flapping flight as a bifurcation in Re_ω. *J. Fluid Mech.* 498, 257–288.

[7] Combes, S. A., Daniel, T. L., 2001. Shape, flapping and flexion: wing and fin design for forward flight. *J. Exp. Biol.* 204, 2073–2085.

[8] Dickinson, M. H., Farley, C. T., Full, R. J., Koehl, M. A. R., Kram, R., Lehman, S., 2000. How animals move: An integrative view. *Science* 288, 100–106.

[9] Dimock, G., Selig, M., 2003. The Aerodynamic Benefits of Self-Organization In Bird Flocks, in *41st AIAA Aerospace Sciences Meeting and Exhibit*, Reno, NV, Paper No. AIAA 2003–0608.

[10] Eldredge, J. D., 2005. Efficient tools for the simulation of flapping wing flows, in *43rd AIAA Aerospace Sciences Meeting*, Reno, NV, Paper No. AIAA 2005–0085.

[11] Gill, P. E., Jay, L. O., Leonard, M. W., Petzold, L. R., Sharma, V., 2000. An SQP method for the optimal control of large-scale dynamical systems. *J. Comp. Appl. Math.* 20, 197–213.

[12] Junge, O., Marsden, J. E., Ober-Blöbaum, S., 2005. Discrete optimal control, preprint.

[13] Kanso, E., Marsden, J. E., 2005. Optimal motion of an articulated body in a perfect fluid, preprint.

[14] Kanso, E., Marsden, J. E., Rowley, C. W., Melli-Huber, J., 2005. Locomotion of articulated bodies in a perfect fluid. *J. Nonl. Sci.*, in press.

[15] Kelly, S. D., 1998. The mechanics and control of robotic locomotion with applications to aquatic vehicles. Ph.D. thesis, California Institute of Technology.

[16] Liao, J. C., Beal, D. N., Lauder, G. V., Triantafyllou, M. S., 2003. Fish exploiting vortices decrease muscle activity. *Science* 302, 1566–1569.

[17] Marsden, J. E., 1992. *Lectures on Mechanics*. Vol. 174 of London Math. Soc. Lecture Note Ser. Cambridge University Press.

[18] Marsden, J. E., Ratiu, T. S., 1999. *Introduction to Mechanics and Symmetry*. Vol. 17 of Texts in Applied Mathematics. Springer-Verlag, New York.

[19] Newman, J. N., 1977. *Marine Hydrodynamics*. Vol. 145. MIT Press, Cambridge, MA.

[20] Newton, P. K., 2001. *The N-Vortex Problem: Analytical Techniques*. Vol. 145 of Appl. Math. Sci. Series. Springer-Verlag, Berlin-Heidelberg-New York.

[21] Oh, Y. G., Sreenath, N., Krishnaprasad, P. S., Marsden, J. E., 1989. The dynamics of coupled planar rigid bodies. Part 2: Bifurcations, periodic solutions and chaos. *Dynamics and Diff. Eq'ns* 1, 269–298.

[22] Radford, J., 2003. Symmetry, reduction and swimming in a perfect fluid. Ph.D. thesis, California Institute of Technology.

[23] Saffman, P. G., 1967. The self-propulsion of a deformable body in a perfect fluid. *J. Fluid Mech.* 28, 385–389.

[24] Serban, R., Petzold, L. R., 2001. COOPT - a software package for optimal control of large-scale differential-algebraic equation systems. *Mathematics and Computers in Simulation* 56, 187–203.

[25] Shapere, A., Wilczek, F., 1989. Geometry of self-propulsion at low Reynolds number. *J. Fluid Mech.* 198, 557–585.

[26] Shashikanth, B. N., Marsden, J. E., Burdick, J. W., Kelly, S. D., 2002. The Hamiltonian structure of a 2D rigid circular cylinder interacting dynamically with n point vortices. *Phys. of Fluids* 14, 1214–1227.

[27] Spedding, G. R., 2003. Comparing fluid mechanics models with experimental data. *Phil. Trans. R. Soc. Lond. B* 358, 1567–1576.

[28] Sreenath, N., Oh, Y. G., Krishnaprasad, P. S., Marsden, J. E., 1988. The dynamics of coupled planar rigid bodies. Part 1: Reduction, equilibria and stability. *Dyn. and Stab. of Systems* 3, 25–49.

[29] Walker, J. A., Westneat, M. W., 1997. Labriform propulsion in fishes: kinematics of flapping aquatic flight in the bird wrasse *Gomphosus varius* (Labridae). *J. Exp. Biol.* 200, 1549–1569.

[30] Zhang, F., Leonard, N., 2005. Generating Contour Plots using Multiple Sensor Platforms, in *Proc. of 2005 IEEE Swarm Intelligence Symposium*, 309–314.